Available online at www.sciencedirect.com
ScienceDirect
Catalysis Today 126 (2007) 135–142
CATALYSIS TODAY
www.elsevier.com/locate/cattod

Operando studies of desorption, reaction and carbonate formation during CO oxidation by Au/TiO_2 catalysts

Jason C. Clark, Sheng Dai, Steven H. Overbury *

Chemical Sciences Division, Oak Ridge National Laboratory, Oak Ridge, TN 37831-6201, USA

Available online 28 November 2006

Abstract

Gas transient methods have been used to probe reaction pathways in catalytic CO oxidation under *operando* conditions. A low dead volume reactor is described, which permits monitoring of surface reaction species by repetitive FTIR while using mass spectrometry to continuously monitor reaction products and conversion throughout transient gas switching. CO desorption rates are measured from an active Au/TiO_2 catalyst under He and CO_2 and are consistent with literature values for CO desorption from Au single crystals and Au films on TiO_2. The rate of the reactive removal of adsorbed surface $CO_{(a)}$ was used to determine a turnover frequency of about 0.043 s^{-1} for CO oxidation on the Au particles, comparable to the rate obtained in a steady state flow reactor. Gas switching is used to investigate the storage of oxygen on the catalyst. It is found that following O_2 exposure, the amount of adsorbed active oxygen is either undetectably small, less than 3.1 μmoles O/g_{catal}, or it desorbs very rapidly at 298 K. Although storage of oxygen is very ineffective on this catalyst, CO_2 is stored by its dynamic interaction with the support to form carbonates or bicarbonates causing slow removal of product CO_2 from the reactor bed. These results are summarized by a scheme describing the pathways for CO oxidation.

Keywords: *Operando* conditions; Desorption; CO oxidation

1. Introduction

Much interest in supported Au nanoparticles has recently arisen due to a demonstrated size effect when these materials are used as catalysts, especially with respect to low temperature CO oxidation. To date, much of the work focused on Au catalysis has been based upon characterization of the structure and oxidation state of the Au particles, the effect of particle size on activity, the nature and effects of the support, preparation conditions, and the effects of impurities and water upon the overall catalytic performance [1,2]. Although there have been several experimental studies of the adsorption of CO on Au catalysts, there has been less work performed to probe surface species under actual reaction conditions by *operando* spectroscopic methods.

A promising variation on *operando* spectroscopy is the application of transient reaction conditions which provide information about reaction pathways by applying an abrupt perturbation to the reactants or to the reactant stream concentration. Shannon and Goodwin have described the steady state isotopic transient kinetic analysis (SSITKA) technique, which makes use of isotopic switching under otherwise steady state conditions to learn surface residence times [3]. This method has been applied to study the intrinsic turnover frequency (TOF) of Au catalysts during CO oxidation reactions [4]. Additionally, it has been used to explore the effect of Au particle size and Cl^- concentration upon the number of active intermediates and the intrinsic site activity [5]. SSITKA experiments in combination with FTIR can be used to monitor surface species throughout the reaction switch to study CO_2 reforming of methane on Rh catalysts [6]. This technique was also used in non-steady state gas switches or pulsing experiments to study reaction pathways in reforming and CO + NO reactions [7,8]. This general approach has been used by Daturi and co-workers to study reduction pathways, active sites, intermediate species and by-products in NOx traps [9,10] as well as for selective catalytic reduction of NOx [11]. More recently, this approach has been applied to Au catalysts to investigate reaction intermediates in CO oxidation and water gas shift reactions [12,13]. Another transient reaction technique,

* Corresponding author. Tel.: +1 865 574 5040; fax: +1 865 576 5235.
E-mail address: overburysh@ornl.gov (S.H. Overbury).

0920-5861/$ – see front matter © 2006 Elsevier B.V. All rights reserved.
doi:10.1016/j.cattod.2006.10.008

temporal analysis of products (TAP) has also been applied to study Au catalysts [14]. Although information about diffusion and support effects was obtained, this method cannot be considered to be an *operando* method.

In the following, we apply transient techniques to probe aspects of the reaction pathways including desorption, oxygen storage, reaction rates and the role of carbonates during CO oxidation reactions using supported Au nanoparticles as a catalyst.

2. Experimental

2.1. Catalyst

Supported gold catalyst (Au/TiO_2) was provided by the World Gold Council (Lot No. 02-5) and was used as provided. The catalyst, which will be referred to as WGC, was prepared by deposition–precipitation onto TiO_2 (Degussa P-25 Lot. No. P1S-2529 sample # 2124) and calcined at 300 °C and had Au loading of 1.47 wt% as determined by ICP analysis. The average particle size was reported to be 3.7 nm as determined by TEM. Although not measured, such a particle size implies a dispersion of about 25–30%. For comparison with this catalyst, experiments were performed with Au-free TiO_2 (P-25) used without any pre-treatment.

2.2. Transient analysis system for operando spectroscopy

Experiments were performed under transient flow conditions brought about by gas switching through a reactor containing a catalyst pellet. Transients were performed using an upstream switching valve and flow rates were controlled with mass flow controllers (see Supplementary Material). During the transients the FTIR spectrum of the pellet and the composition of the gas flowing out of the reactor were continuously monitored. Infrared (IR) spectroscopy was conducted in a home-made brass IR cell fitted with CaF_2 windows in a Nicolet Nexus 670 FTIR spectrometer using an MCT/A detector with a KBr beam splitter. In a typical experiment, FTIR spectra were obtained at 5 s intervals and summing four scans for each spectrum with a spectral resolution of 4 cm^{-1}. Prior to data collection, samples pellets were heated to 333 K under a flowing UHP He atmosphere to remove loosely bound surface species. After this treatment, a background spectrum was collected using 256 scans and 4 cm^{-1} resolution (see Supplementary Material for a typical background spectrum). Although higher temperatures are needed to completely remove all carbonate species, this treatment provided a stable FTIR background that showed no changes with time under inert conditions. Difference spectra were obtained by subtracting the background from subsequent spectra and are reported herein. Gases leaving the reactor cell were analyzed using a gas sampling quadrupole mass spectrometer (Pfeiffer-Balzer Omnistar) equipped with a 1 m long gas sampling capillary followed by an apertured entrance into the turbo-pumped quadrupole chamber. The temperature of the IR reactor cell was controlled using a ThermoNESLAB RTE circulating bath/cooler containing 1:1 (v/v) ethylene glycol/water mixture. A controlling thermocouple was embedded in the reactor cell near the catalyst such that the temperature of the catalyst was controlled in the 243–363 K range.

Self-supporting pellets of untreated WGC or TiO_2 were made by lightly pressing ~45 mg of catalyst and these were placed into the reactor for IR studies. Based upon weight loading and dispersion such pellets expose about 3.4 μmoles of total Au and 0.92 μmoles of surface Au. Gases were provided by Air Liquide and were as follows: 2% CO/2% Ar/He, 2% O_2/He, and 2% CO_2/He and UHP He. A manifold of valves including a four-way and six-way switching valves were used for abrupt switching or pulsing of the gases through the reactor. [15] A pair of two-way valves could be used to allow the gas to bypass the reactor. Typically, the total flow rates were fixed at 25 cm^3/min.

3. Results and discussion

3.1. Reactor properties

In order to observe fast surface transients, it is required that the reactor has a low dead volume, and a reactor was constructed with this as a major design criterion. The reactor consists of two brass blocks, which can be bolted together (Fig. 1), each with a center hole to accommodate CaF_2 cylinders. The two CaF_2 cylinders (Fig. 1A) slip through internal O-rings and can be adjusted to clamp the sample wafer between them when the blocks are bolted together. In this fashion, the gas phase pathlength is largely eliminated. An outer O-ring between the blocks (Fig. 1B) defines the narrow region of turbulent gas flow within the reactor. Gas is introduced through a hole on one block below the wafer and is removed

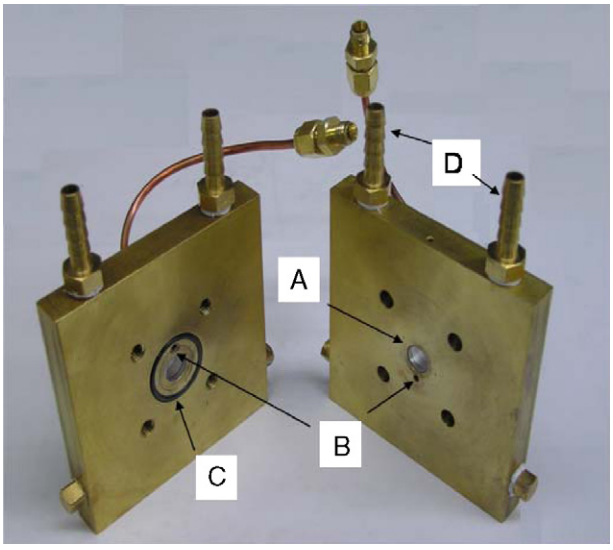

Fig. 1. Photograph of the two halves of the reaction cell. A cylindrical, CaF_2 rod (A) slides through internal O-rings located on both halves. A sample pellet is held between the CaF_2 rods when the two halves are bolted together. Gas flows into and out of the cell through small holes (B) and is contained within the volume sealed by the O-ring (C). Chilling fluid is circulated through ports in the body of both halves (D).

from a hole above the wafer in the other block (Fig. 1C). The reactor volume surrounding the wafer is theoretically $<0.05\ cm^3$.

In order to test the gas transients of the cell, the rate of gas elution out of the reactor was monitored by performing a gas switch from 2% Ar in He to pure He. This time profile of the decrease in the Ar concentration in the product stream after the switch provides information about the time resolution of the gas transient. Such a measurement was performed through the reactor and was found to exhibit a half-width on the order of 5 s, much broader than expected. Considering the theoretical dead volume, V_r, and the flow rate ($F = 25\ cm^3$ /min) the expected width should be approximated by V_r/F or about 0.1 s. For comparison a similar switch was performed through the sample bypass. In this latter case the effects of turbulent mixing in the reactor is eliminated and the results test the response of the mass spectrometer sampling system. The results from two such gas switches are shown in Fig. 2. The normalized Ar concentration profile, $c(t)$, through the bypass can be fit well to an equation which contains an exponential decrease combined with a diffusive component in the source term:

$$\frac{dc}{dt} = -c\left(\frac{F}{V}\right) + c_0\left(\frac{F}{V}\right)\exp\left(-\frac{(t-t_0)^2}{2\sigma^2}\right) \quad (1)$$

where σ is a parameter describing the mixing at the interface following the gas switch. A fit to this equation is included in Fig. 2 using σ of 2.1 s and V/F of 0.31 s. When switched through the reactor an additional broadening is observed, which is associated with the time required to flush out the reactor. A small contribution (about 2%) from a slow tail ($t_{1/2}$ of 24 s) is observed in the concentration profile. Adding this exponential component to the solution to (1) gives the fitted curve shown in Fig. 2. The conclusion is that for the reactor configuration most of a non-interacting gas can be eluted from the reaction cell in less than a few seconds, the time resolution limit of the mass spectrometer sampling system.

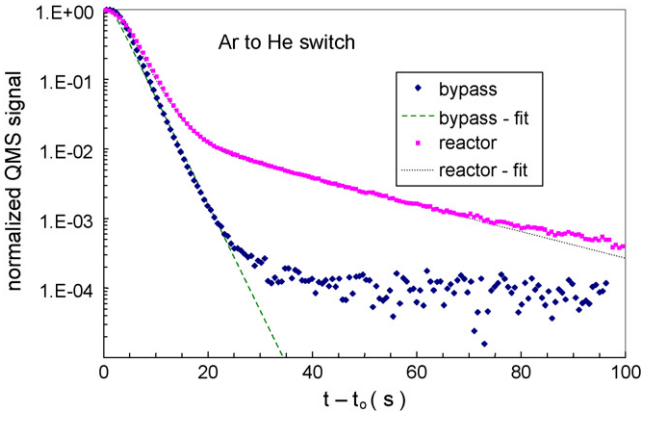

Fig. 2. Response of the mass spectrometer following a switch from 2% Ar/He to pure He when the flow is diverted through a bypass is compared with that when the gas flows through the reactor. The flow through the bypass is fitted to Eq. (1) (see text) and reflects the response time and diffusive broadening of the gas boundary in the gas lines and the mass spectrometer sampling system. The slightly broader response through the reactor demonstrates fast purging of most gas from the reactor and a slower purge of about 2% of the gas.

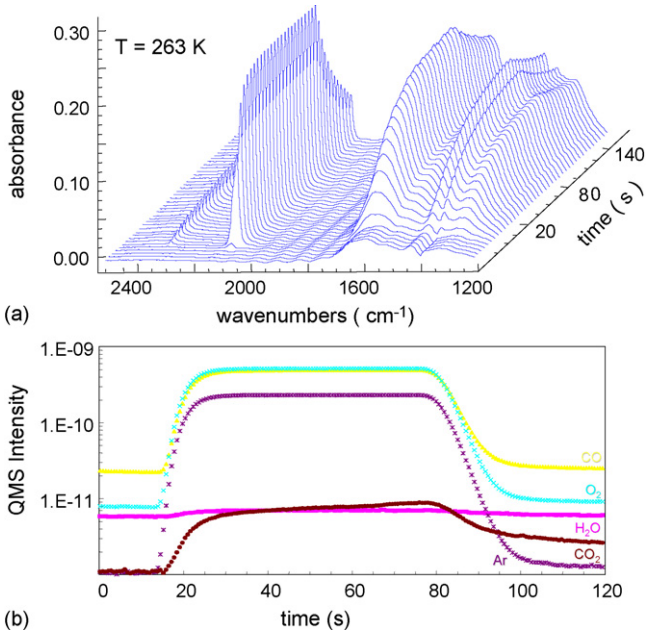

Fig. 3. (a) FTIR and (b) QMS response from switching from He to a reactive mixture of 1% CO and 1% O_2 in He over WGC at 263 K.

Illustrative FTIR and QMS results obtained simultaneously following switching of reactant mixture over the Au catalysts are shown in Fig. 3. In this case, He was flowed (25 cm^3/min) across the sample for several minutes while the sample was cooled to 253 K to permit purging and desorption from the catalyst. After this purge, a reference IR spectrum was obtained just before switching from He gas to the reactant mixture consisting of 2% CO/2% Ar/He (12.5 mL/min) and 2% O_2/He (12.5 mL/min) at time $t = 0$. This mixture was flowed for 60 s before switching back to He. The QMS exhibits sharp changes as the reactant gas front passes by the gas sampler and the CO_2 response indicates catalytic conversion. Under these conditions the FTIR spectrum shows an abrupt build-up of adsorbed species characterized by peaks near 2100 cm^{-1} (adsorbed $CO_{(a)}$), 2343 cm^{-1} (adsorbed $CO_{2(a)}$) and region from 1250 to 1700 cm^{-1} exhibiting several broad peaks due to surface bound carbonates and bicarbonates [15].

3.2. Desorption of CO

Total CO desorption rates from WGC were probed using gas switching techniques. These experiments were performed by flowing CO for an extended period and then switching abruptly to He (in some cases O_2 or CO_2). Fig. 4a shows the region in the FTIR spectrum where a signal corresponding to $CO_{(a)}$ is expected following a switch from CO to He recorded at 248 K. Before the switch, while flowing CO (2% CO in He at ambient pressure), a peak is observed at 2102 cm^{-1} due to adsorbed $CO_{(a)}$. The absence of vibrational–rotational peaks from gas phase CO demonstrates the short gas phase pathlength resulting from the sample holder design. The observed peak position is

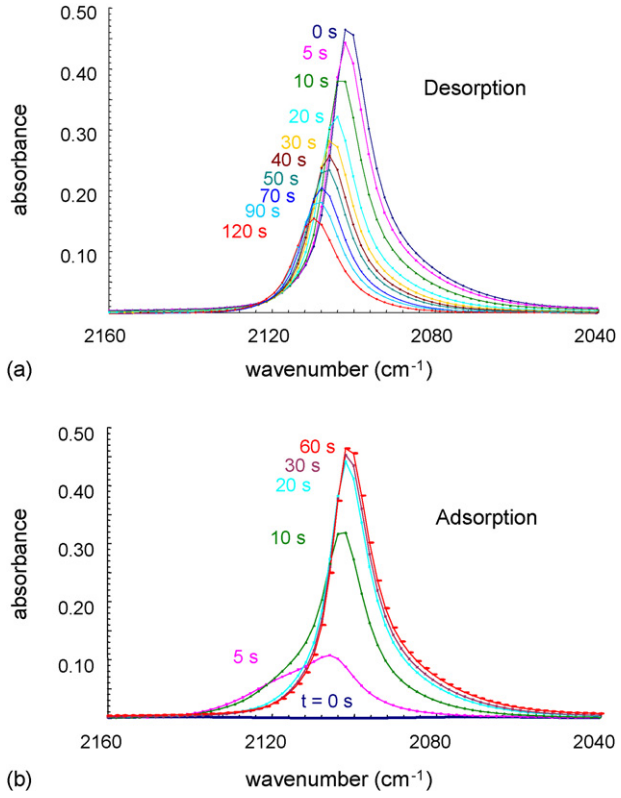

Fig. 4. (a) FTIR spectra showing the desorption of $CO_{(a)}$ from WGC after a switch from 2% CO in He to pure He at 248 K. (b) FTIR spectra showing the adsorption of $CO_{(a)}$ onto WGC after a switch from pure He to 2% CO in He at 248 K.

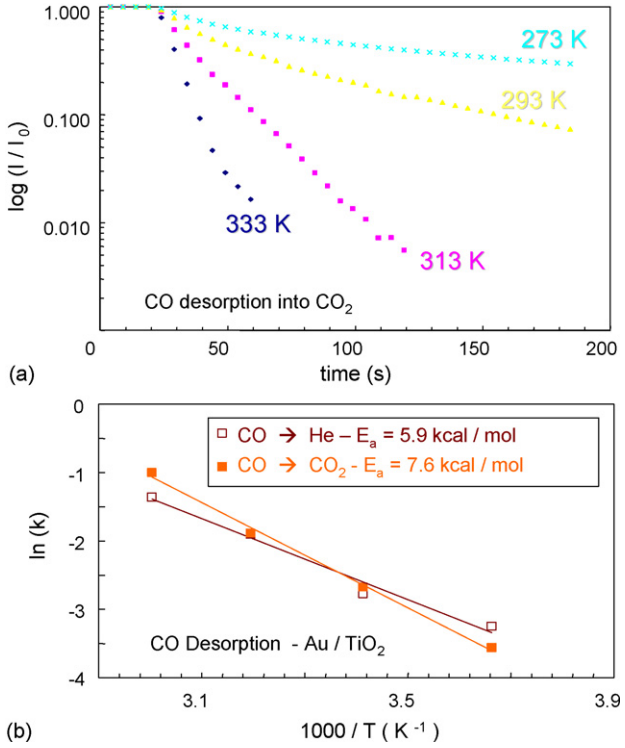

Fig. 5. (a) Logarithmic plot of the normalized integrated intensity of the FTIR signal at approximately 2105 cm^{-1} vs. time used to determine rates of desorption at various temperatures. (b) Arrhenius plot derived from the rates of desorption of $CO_{(a)}$ from WGC.

characteristic of high coverage, linear adsorbed CO on Au particles as has been observed in single crystal studies of Au [16–19] and on Au/TiO_2 catalysts [20–22]. Immediately following the switch to He, the peak shows a decline in intensity due to desorption of $CO_{(a)}$ from supported Au nanoparticles, accompanied by a shift to higher frequency (2110 cm^{-1}) after desorbing for 2 min. Desorption is faster at higher temperatures (not shown) leading to lower coverages (after 2 min) accompanied by a peak shift to frequencies as high as 2114 cm^{-1}. Such red shifts in peak position with increasing coverage on Au single crystals have been observed previously [17,23,24] and are attributed to a combination of competing interactions [17]. We do not believe that the two states evolve from adsorption on Au of two different oxidation states, since our XANES results indicate that Au on TiO_2 supports is essentially completely in the reduced state [25]. Similar experiments were previously performed on Au-free TiO_2 and it was determined that CO does not adsorb at temperatures as low as 253 K, even in the presence of O_2 based on the absence of signal in the FTIR near 2100 cm^{-1} [15].

Assuming that the CO peak intensity is proportional to coverage, an approximation that may only be true at low coverage [26], logarithmic plots of the coverage versus time curves were used to obtain a rate of desorption. This assumption is approximately true in this instance because exposure of the catalyst to flowing CO or CO_2 resulted first in a continuous increase in FTIR intensity followed by a stable maximum intensity once the surface was saturated with the adsorbing gas. A typical result is shown in Fig. 5a for desorption of CO into a CO_2 ambient following a switch from CO to CO_2. Approximately exponential intensity decrease was observed following the gas switch, the negative slope, k, of which is the desorption rate. Repeating this rate measurement for several temperatures leads to the Arrhenius plots shown in Fig. 5b. Two data sets are shown, one in which CO is desorbed into He and the second in which CO is desorbed into CO_2. Both sets lead to comparable desorption rates and apparent activation energies of 5.9 and 7.6 kcal/mole for desorption into He and CO_2, respectively. These values match well with heats of adsorption measured from CO adsorption isotherms on Au(1 1 0) surface which is 7.8 ± 1.3 kcal/mole in the high coverage limit [27]. It also matches measurements of high coverage limit for Au particles, estimated to be about 3 nm in diameter, grown on TiO_2 films [17]. The close correspondence with Au single crystal data for the FTIR peak positions, the coverage dependent shifts and the desorption/adsorption energies together indicate that the CO adsorption is occurring on the Au particles and not the support. Furthermore, since the rates are independent of whether CO desorption occurs in the presence of CO_2 or He, CO_2 does not enhance CO desorption.

The $CO_{(a)}$ peak shape at low to intermediate coverages depends upon whether the $CO_{(a)}$ is increasing (adsorbing) or decreasing (desorbing or reacting). Adsorption experiments were performed by flowing He (or in some cases O_2 or CO_2) for an extended period and then switching abruptly to CO. During adsorption (Fig. 4b) the CO FTIR signal suggests two co-existing

species: one species at 2116 cm^{-1} which populates first and then diminishes with time, and a second at 2106 cm^{-1} which grows and red shifts to 2102 cm^{-1} with increasing time. This behavior was also seen at other temperatures and occurred whether the adsorption was preceded by He or O_2. During desorption (Fig. 4a) the single sharp peak observed at saturation shifts continuously toward lower frequency. Similar behavior was observed if CO was reacted away by switching to O_2 (instead of He), although the loss of surface $CO_{(a)}$ was more rapid compared to desorption alone. The different peak evolutions for adsorption compared to desorption indicates that these two processes are governed by different dynamics. This result can be explained by a clustering model where increasing coverage of $CO_{(a)}$ first adsorbs on clean Au particles in widely spaced atop sites (2116 cm^{-1}), followed by nucleation of denser $CO_{(a)}$ islands (2106 cm^{-1}) which grow (with frequency shift) and dominate at higher coverage. Desorption (or reaction) occurs *primarily* from island edges causing a gradual frequency shift as the islands shrink. Apparently, clustering of CO and/or the distribution of the two different $CO_{(a)}$ species (island versus isolated) is not at equilibrium but depends upon whether the sites are populating or depopulating.

3.3. Storage of CO and reactive oxygen

It is of interest to consider the relative rate of desorption of surface CO compared to the rate of its reaction on the surface. Such information can be obtained by conducting a direct switch or a delayed switch from CO to O_2. In a direct switch, CO is flowed for a period of time and then the gas stream is switched abruptly to O_2 and reaction of surface $CO_{(a)}$ begins. In a delayed switch, the CO flow is switched to He, which flows for a timed interval before O_2 is switched into the reactor. $CO_{(a)}$ desorbs during the He interval and then reaction commences when the oxygen reaches the reactor zone. In a special case of a long He interval, no oxygen reaches the reactor before all CO desorbs. The results of such experiments are shown in Fig. 6 where the intensity of the $CO_{(a)}$ peak (2102–2110 cm^{-1}) is monitored following a direct switch, and for two delayed switches with delays of 10 and 15 s, and for CO desorption where the He interval is longer than 100 s.

The results clearly indicate that this $CO_{(a)}$ is the reactive species in the reaction and that at 248 K the reaction rate is competitive with or faster than the desorption rate. Because of the relatively slow desorption rate, CO may be stored briefly on the surface when oxygen is not present. From the gas flow rate and O_2 concentration, the arrival rate of O_2 is about 0.4 μmoles/s compared to a total of 0.9 μmoles of surface Au in the pellet. If CO is adsorbed at a ratio of about 1:1 on surface Au, enough oxygen to oxidize all CO could reach the Au in about 1 s if diffusion through the pellet is not limiting. The observed exponential rate of decrease can be described by time constant of about 0.053 s^{-1} which results from the sum of desorption and reaction rates. Subtracting the observed desorption rate yields a reaction rate of about 0.043 s^{-1} which can be equated with a TOF. Note that this is a true turnover frequency since it is relative to *only* the active Au sites, that is, the sites which adsorb CO. This may be compared with the TOF measured in a flow reactor and previously reported at 235 K to be 0.023 s^{-1}, a TOF based upon the total Au in the sample [28].

These results suggest a method to determine the amount of oxygen that may be stored on the surface and/or its persistence on the surface. Although adsorbed oxygen cannot be observed on the surface by FTIR, its presence may be detected indirectly by its effect on CO uptake. Experiments to detect such oxygen are shown in Fig. 7 performed at 298 K where CO oxidation rate is rapid. In this case O_2 is flowed for 60 s prior to a direct switch to CO. This is to be compared to a simple CO uptake in which only He is flowed prior to a switch to CO, i.e. in which there is no pre-adsorbed oxygen. In both cases, the onset of CO uptake is referenced relative to the time that the switching valve is activated. This timing was used since there is no other non-reacting, FTIR detectable gas adsorbing in the CO stream, and so there is no FTIR time marker. If reactive oxygen remains on the surface, a delay in the CO uptake is anticipated compared to a CO uptake without pre-adsorbed oxygen. This effect is

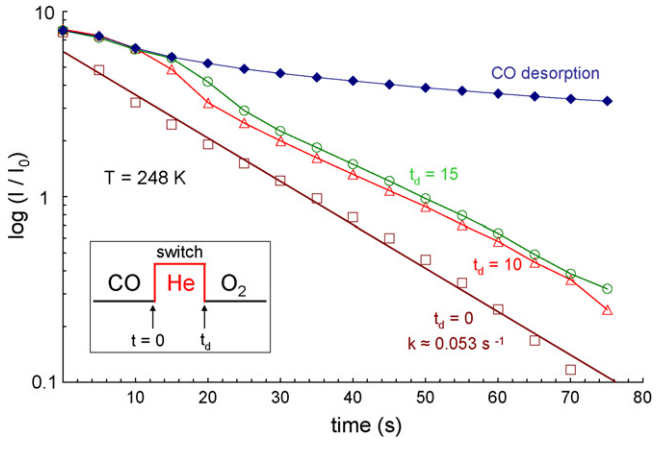

Fig. 6. The integrated intensity of the $CO_{(a)}$ FTIR feature located near 2105 cm^{-1} is shown as a function of time after a direct or delayed switch to O_2.

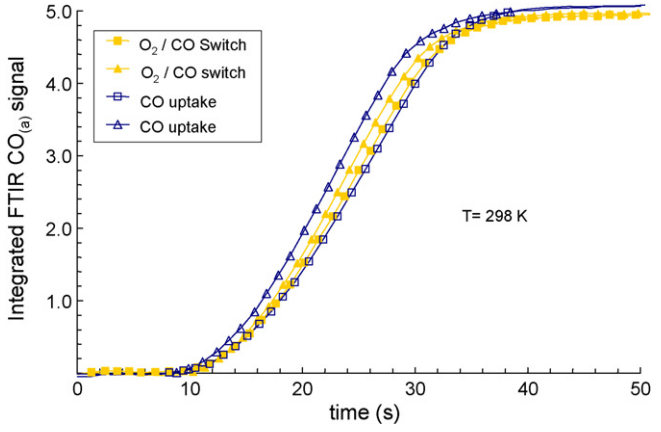

Fig. 7. The integrated intensity of the $CO_{(a)}$ FTIR feature located near 2105 cm^{-1} is shown as a function of time after switching from O_2 to CO or from He to CO (CO uptake). The results of two different runs for each type of switch are shown.

expected to occur because the first CO to adsorb will react quickly rather than remain as detectable $CO_{(a)}$. A smaller CO concentration (0.44%), a larger pellet (52 mg) and a faster FTIR sampling rate (1 s) were used to increase sensitivity in this experiment. Prior to each switch, the sample was warmed to 333 K in He for approximately 1 h to remove $CO_{2(a)}$ and carbonates before cooling down to 298 K in He to perform the switch.

Two such switches of each type are shown in Fig. 7. Within the experimental fluctuation in time for the gas front to reach the reactor, about ±2 s, there is no measurable delay in CO uptake following oxygen pre-adsorption. Since CO arrives at a rate of 0.08 μmoles/s and there is 1.0 μmoles of surface Au, CO should react with oxygen atoms adsorbed on the Au surface at the rate of up to 0.08 monolayers/s. Delays of up to 12 s are expected for monolayer of adsorbed O coverage or 24 s for a monolayer of O_2 adsorbed on the Au surface. Even greater delays may be expected if the TiO_2 support retains reactive oxygen. The actual delay of less than 2 s implies that either less than 3.1 μmoles O/g_{catal} is stored anywhere on the catalyst surface or the oxygen desorption rate at 298 K is rapid compared to the CO arrival rate.

3.4. Surface carbonate species

As shown in Fig. 3, as $CO_{(a)}$ reacts with oxygen to form $CO_{2(a)}$, a build-up of several peaks are observed in the FTIR spectra between 1800 and 1200 cm^{-1} that may be assigned to carbonate and bicarbonate species. Most of these features are also observed for the pure TiO_2 and have been assigned previously [21,29,30]. The role, if any, these species play in the reaction pathway is not yet fully understood.

Experiments were conducted in which either CO_2 or a mixture of CO and O_2 were switched into the reactor, following an extended period of flushing in He at a fixed temperature. Both the WGC and TiO_2 were used and spectra obtained following exposure (for about 1 min) at 263 K are shown in Fig. 8. As was previously reported [15], a mixture of CO and O_2 does not interact with TiO_2 to form carbonates detectable by FTIR. However, exposure of TiO_2 to CO_2 resulted in the observation of immediate signals in the FTIR that were consistent with the formation of carbonate species. Additionally, these signals grew in intensity with increasing exposure to CO_2 indicating a build-up of carbonate species on the surface which results from the interaction of CO_2 with TiO_2. Furthermore, the presence of gold nanoparticles is not necessary for their evolution. Similar experiments conducted on the WGC shows build-up of the carbonate features whether it is exposed to CO_2 or to the reaction mixture. In the case of the mixture, the carbonate features are the result of adsorption of CO_2 produced catalytically from the reaction over the Au surface. The FTIR spectra have similar features whether exposed to CO_2 or to the mixture, but the integrated intensity of the carbonate species that evolved when WGC was exposed to CO_2 was approximately two times greater than when a mixture of CO and O_2 was used. This intensity differences was attributed to a greater concentration of CO_2 present when CO_2 gas is used compared to the when the CO_2 results from CO oxidation.

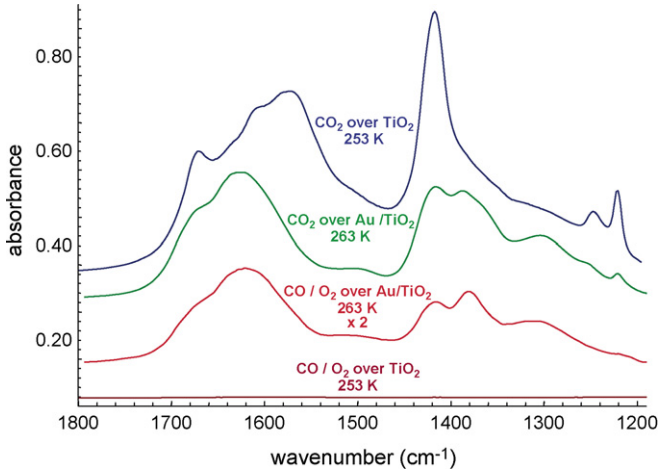

Fig. 8. FTIR signals corresponding to carbonate species on the WGC or on TiO_2 (P-25) resulting from an exposure to either CO_2 or a CO/O_2 reactive gas mixture.

Differences between the WGC and the TiO_2 are apparent in the spectra compared in Fig. 8 and indicate differences in the relative amounts of the various carbonate species. However, the relative intensities of the features were observed to depend considerably upon the temperature at which the adsorption was carried out. These species are difficult to remove from TiO_2 and WGC and since the spectra were accumulated by subtracting acquired spectra from a background spectrum obtained at the start of a switch, the initial state affects the subsequent evolution. Previously, it was reported that water present on the surface of TiO_2 is almost certainly a factor in controlling the relative amounts of surface bound carbonates [31]. Dissimilarities between these spectra are probably due to differences in the details of pre-treatment. Careful evaluation of differences in the spectra caused by subtle changes in the amount of water present and pre-treatment conditions was not carried out.

3.5. Desorption of CO_2

Attempts to measure CO_2 desorption rates using similar methods to those described in Section 3.2 demonstrated important differences between the behavior of CO_2 and CO with the catalysts. Adsorption of CO_2 onto the WGC produces a sharp peak at 2343 cm^{-1} as seen in Fig. 9a, with a clear absence of gas phase peaks. The position of this peak, assigned to adsorbed $CO_{2(a)}$ is independent of coverage, and occurs at the same frequency when the Au-free TiO_2 is used in the reactor. Desorption of the $CO_{2(a)}$ is slower than for CO at comparable temperatures and appears to have both a fast and a slow component of desorption (Fig. 9b). The slow component is difficult to determine at higher temperature due to lower signal intensities and issues with subtracting background spectra, for example Fig. 9b. Attempting to fit an exponential rate to the initial faster decrease leads to a very low activation energy of around 1–2 kcal/mole for both the WGC and the TiO_2 whether desorbing into He or into CO (Fig. 9c). Such low activation

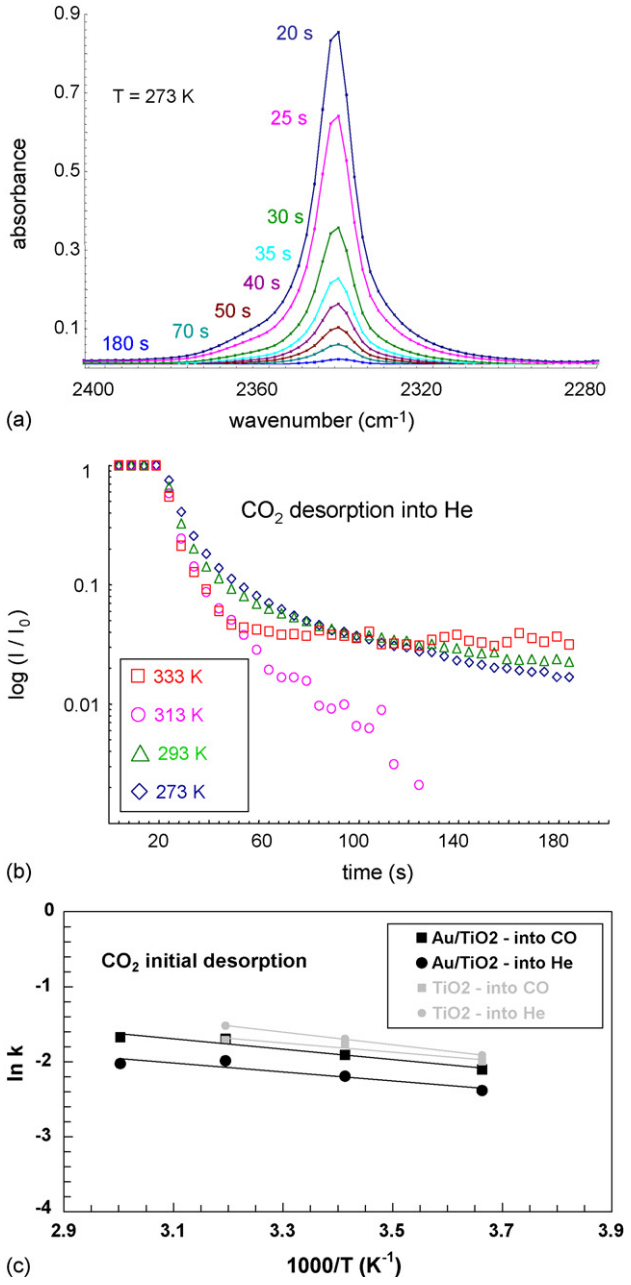

Fig. 9. (a) FTIR spectra showing the desorption of $CO_{2(a)}$ from WGC after a switch from 2% CO_2 in He to pure He at 273 K. (b) Logarithmic plot of the integrated intensity of the FTIR signal at approximately 2345 cm^{-1} vs. time at various temperatures. (c) Arrhenius plot derived from the determined rates of desorption of the fast component of $CO_{2(a)}$ desorption from WGC and from TiO_2 into He or CO.

energies obtained from the fast component are consistent with a diffusion controlled removal process typified by repetitive desorption/readsorption process. The intensity of the $CO_{2(a)}$ peak at saturation depends upon temperature but roughly comparable intensities are obtained whether TiO_2 or the WGC is used. The similar peak positions, intensities and activation energies for TiO_2 and WGC suggest that the $CO_{2(a)}$ is primarily present on the support. However, it is not possible to eliminate that a comparably adsorbed $CO_{2(a)}$ forms on the Au particles and rapidly mixes with the support.

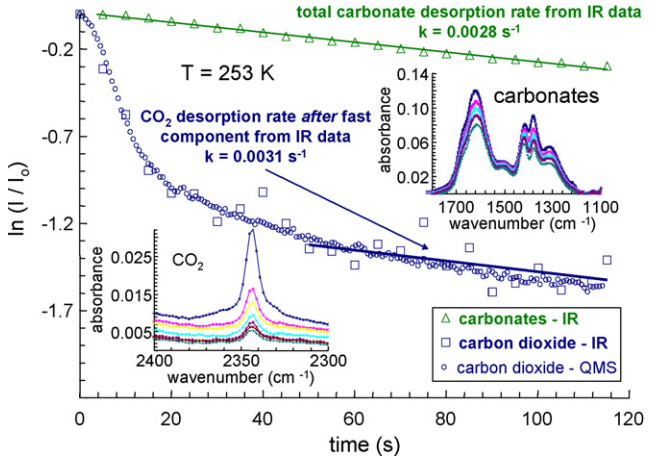

Fig. 10. FTIR signal from the carbonate region and from the $CO_{2(a)}$ are compared as a function of time after switching from reaction mixture (CO/O_2) to He across the WGC. In addition, the CO_2 QMS signal recorded downstream is shown, offset in time relative to the FTIR to account for the delay required for the gas front to reach the downstream inlet to the QMS gas sampler. All intensities are normalized to unity at $t = 0$.

The reason for the two-component desorption can be linked to the effects of carbonate species build-up on the surface. The dynamics of surface CO_x species were examined by comparing the desorption rates of $CO_{2(a)}$ and the loss of carbonate from the Au catalyst. Fig. 10 shows this comparison following switches from reaction CO/O_2 to He for the WGC catalysts at 253 K. During the exposure to the reaction mixture, both carbonates and $CO_{2(a)}$ build-up on the surface as typified in Fig. 3. When the reaction mixture is switched to He, the FTIR signals from both the carbonates and the $CO_{2(a)}$ begin to decrease as shown in Fig. 10. The concentration of the downstream CO_2 also drops and matches closely the decrease in the surface coverage of $CO_{2(a)}$. This close correlation was observed at four different temperatures between 253 and 283 K, and indicates that the surface concentration of $CO_{2(a)}$ is in equilibrium with the gas phase. After the initial fast decrease in the CO_2 concentration and surface $CO_{2(a)}$ (lasting about 20 s as shown in Fig. 10), the rate of decrease slows considerably and the rate of the total CO_2 disappearance matches the rate determined for the exponential loss of total surface bound carbonates species as indicated by FTIR. This correlation suggests some of the carbonate species are decomposing to CO_2 which then equilibrates with the catalyst surface. Thus, the carbonates serve as a storage medium and source for product CO_2. Even though the carbonates are spectators, they alter the rate at which CO_2 is evolved from the reactor. Any non-steady state measurement of CO conversion obtained by measurement of CO_2 evolved must consider this pathway.

4. Conclusions: pathways for CO oxidation on WGC

Based upon these studies, the pathways for CO oxidation can be concluded and are shown schematically in Scheme 1. It was shown previously [15] that non-competitive binding exists between CO and O_2 suggesting distinct adsorption sites. This difference in the nature of the interactions of CO and O_2 with

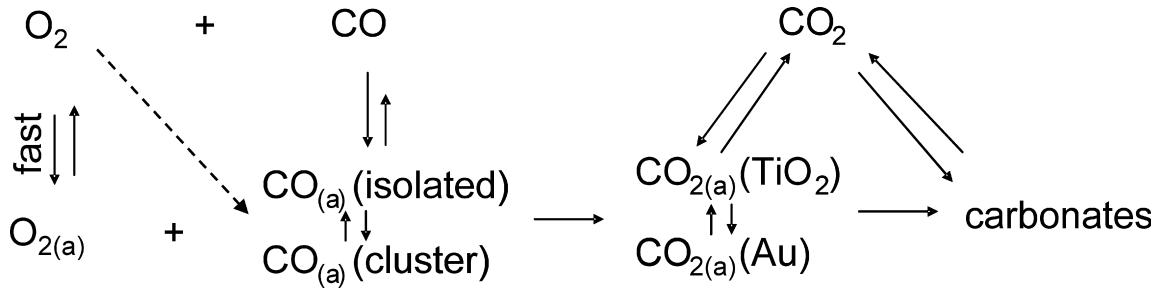

Scheme 1.

WGC became evident in this study and the results mentioned herein suggest that the adsorption of O_2 on WGC either occurs at a very low coverage, or its desorption is very fast. However, we cannot rule out the possibility that adsorbed CO reacts directly with gas phase O_2 via the Eley-Rideal mechanism [32] (dashed line in Scheme 1). In contrast, CO adsorbs on Au nanoparticles readily and the clustering of $CO_{(a)}$ on the surface of these particles into islands (as opposed to isolated adsorbed $CO_{(a)}$ species) depends upon whether the coverage is increasing or decreasing. $CO_{(a)}$ reacts rapidly in the presence of gas phase O_2 to form $CO_{2(a)}$, reacting either with weakly adsorbed $O_{2(a)}$ or directly with gas phase O_2. The product CO_2 can then desorb from the Au particle and interact with the support to form transient carbonate species which then slowly decompose to CO_2. This gas phase CO_2 can now re-adsorb onto the support. This readsorption/decomposition process, indicative of a dynamic equilibrium between adsorbed $CO_{2(a)}$, surface bound carbonate species, and product gas phase CO_2 results in the slow evolution of CO_2 during this reaction compared to other components for this reaction. This description is consistent with the conclusion that the desorption of $CO_{2(a)}$ is the rate limiting step in CO oxidation over WGC [15].

Acknowledgements

Research sponsored by the Division of Chemical Sciences, Geosciences, and Biosciences, Office of Basic Energy Sciences, U.S. Department of Energy, under contract DE-AC05-00OR22725 with Oak Ridge National Laboratory, managed and operated by UT-Battelle, LLC. J.C. is sponsored by an appointment to the Oak Ridge National Laboratory Postdoctoral Research Associates Program administered jointly by the Oak Ridge Institute for Science and Education and Oak Ridge National Laboratory.

Appendix A. Supplementary data

Supplementary data associated with this article can be found, in the online version, at doi:10.1016/j.cattod.2006.10.008.

References

[1] M. Haruta, M. Date, Appl. Catal. A Gen. 222 (1–2) (2001) 427–437.
[2] G.C. Bond, D.T. Thompson, Catal. Rev. -Sci. Eng. 41 (3–4) (1999) 319–388.
[3] S.L. Shannon, J.G. Goodwin, Chem. Rev. 95 (3) (1995) 677–695.
[4] J.T. Calla, R.J. Davis, J. Phys. Chem. B 109 (6) (2005) 2307–2314.
[5] S.S. Pansare, A. Sirijaruphan, J.G. Goodwin, J. Catal. 234 (1) (2005) 151–160.
[6] R.W. Stevens, S.S.C. Chuang, J. Phys. Chem. B 108 (2) (2004) 696–703.
[7] R. Krishnamurthy, S.S.C. Chuang, M.W. Balakos, J. Catal. 157 (2) (1995) 512–522.
[8] S.S.C. Chuang, C.D. Tan, J. Catal. 173 (1) (1998) 95–104.
[9] T. Lesage, C. Verrier, P. Bazin, J. Saussey, M. Daturi, Phys. Chem. Chem. Phys. 5 (20) (2003) 4435–4440.
[10] T. Lesage, C. Verrier, P. Bazin, J. Saussey, S. Malo, C. Hedouin, G. Blanchard, M. Daturi, Topics Catal. 30–31 (1–4) (2004) 31–36.
[11] N. Bion, J. Saussey, M. Haneda, M. Daturi, J. Catal. 217 (1) (2003) 47–58.
[12] J.D. Henao, T. Caputo, J.H. Yang, M.C. Kung, H.H. Kung, J. Phys. Chem. B 110 (17) (2006) 8689–8700.
[13] H. Sakurai, T. Akita, S. Tsubota, M. Kiuchi, M. Haruta, Appl. Catal. A Gen. 291 (1–2) (2005) 179–187.
[14] M. Olea, Y. Iwasawa, Appl. Catal. A Gen. 275 (1–2) (2004) 35–42.
[15] B.K. Chang, B.W. Jang, S. Dai, S.H. Overbury, J. Catal. 236 (2) (2005) 392–400.
[16] R. Meyer, C. Lemire, S.K. Shaikhutdinov, H. Freund, Gold Bull. 37 (1–2) (2004) 72.
[17] D.C. Meier, D.W. Goodman, J. Am. Chem. Soc. 126 (2004) 1892–1899.
[18] Y. Jugnet, F. Aires, C. Deranlot, L. Piccolo, J.C. Bertolini, Surf. Sci. 521 (1–2) (2002) L639–L644.
[19] L. Piccolo, D. Loffreda, F. Aires, C. Deranlot, Y. Jugnet, P. Sautet, J.C. Bertolini, Surf. Sci. 566 (2004) 995–1000.
[20] F. Boccuzzi, A. Chiorino, M. Manzoli, Surf. Sci. 454–456 (2000) 942–946.
[21] F. Boccuzzi, A. Chiorino, S. Tsubota, M. Haruta, J. Phys. Chem. 100 (9) (1996) 3625–3631.
[22] F. Boccuzzi, S. Tsubota, M. Haruta, J. Electron. Spectrosc. Relat. Phenom. 64–65 (1993) 241–250.
[23] A.M. Bradshaw, J. Pritchard, Proc. R. Soc. A 316 (1525) (1970) 169.
[24] C. Ruggiero, P. Hollins, Surf. Sci. 377 (1–3) (1997) 583–586.
[25] V. Schwartz, D.R. Mullins, W.F. Yan, B. Chen, S. Dai, S.H. Overbury, J. Phys. Chem. B 108 (40) (2004) 15782–15790.
[26] H. Pfnur, D. Menzel, F.M. Hoffmann, A. Ortega, A.M. Bradshaw, Surf. Sci. 93 (2–3) (1980) 431–452.
[27] D.C. Meier, V. Bukhtiyarov, A.W. Goodman, J. Phys. Chem. B 107 (46) (2003) 12668–12671.
[28] W.F. Yan, B. Chen, S.M. Mahurin, V. Schwartz, D.R. Mullins, A.R. Lupini, S.J. Pennycook, S. Dai, S.H. Overbury, J. Phys. Chem. B 109 (21) (2005) 10676–10685.
[29] C. Morterra, C. Anna, F. Boccuzzi, Z. Phys. Chem. Neu. Fol. 124 (1981) 211–222.
[30] D.J.C. Yates, J. Phys. Chem. 65 (1961) 746.
[31] K. Tanaka, J.M. White, J. Phys. Chem. 86 (24) (1982) 4708–4714.
[32] C.N. Costa, S.Y. Christoua, G. Georgiou, A.M. Efstathiou, J. Catal. 219 (2) (2003) 259–272.